NUMERICAL AND EXPERIMENTAL INVESTIGATION OF MICROSTRUCTURE EVOLUTION AND MECHANICAL BEHAVIOR OF STEEL IN LASER FORMING

Yajun Fan[1], Zhishang Yang[2], Peng Cheng[1], Keith Egland[2], Y. Lawrence Yao[1]

[1]Department of Mechanical Engineering, Columbia University, New York, NY, 10027, USA
[2]Technical Center, Caterpillar, Inc, Peoria, IL, 61552, USA

Abstract

In laser forming, phase transformation and grain structural evolution in the heat affected zone (HAZ) take place under steep cooling rates and temperature gradients, and have a significant effect on the laser forming process and final mechanical properties of products. In this work, microstructure evolution during laser forming of AISI 1010 steel is experimentally and numerically investigated and the transient constitutive property of phases and grain size are calculated by coupling the thermal history from finite element analysis with a phase transformation kinetic model. Phase volume fraction and grain distribution are predicted. Consequently, the flow stress of material is obtained from the constitutive relationship of the phases, and the laser forming process is modeled considering the effect of work hardening, recrystallization and phase transformation. A series of carefully controlled experiments are also conducted to validate the theoretically predicted results.

1. Introduction

Laser forming is a flexible forming process, during which a laser beam causes local thermal expansion and deformation is obtained by non-uniform release of thermal stresses during cooling. With very fast heating and cooling, laser forming is significantly different from other hot working processes. During laser forming, steep temperature gradients and thermal cycles cause severe microstructural changes in the heat affected zone (HAZ) and fairly high strain and strain rate are also involved; however, melting has to be avoided. Cheng and Yao [1] introduced the methodology of numerical modeling during normal hot working processes such as hot rolling into laser forming of AISI 1012 steel, and the flow behavior of material under steep thermal cycles was modeled considering strain hardening, dynamic recrystallization and phase transformation. The contribution of each phase to flow stresses under different stages, recovery or recrystallization, was calculated. The numerical results agreed very well with the experimental results. However, due to the complexity of the laser forming process and a lack of key material data, the phase transformation and the grain structural evolution occurring during the laser forming process were not fully investigated. Instead, some approximations were made. For example, the phase constitution during $\alpha \rightarrow \gamma$ phase transformation was simplified to be a linear relationship from A_{1ne} temperature to A_{3ne} temperature.

With recent developments in computer simulation of phase transformations and grain structural evolutions based on the fundamental kinetic and thermodynamic theories, it is possible to introduce these techniques to describe the particular laser forming process. In the present research, by combination of experiments and modeling, we seek to quantitatively understand the kinetics of phase transformation and grain structural evolution during laser forming of AISI 1010 steel and their influence on flow behavior and deformation (in particular, the $\alpha \rightarrow \gamma$ phase transformation during rapid heating, the decomposition of γ phase during rapid cooling, and the recrystallization). During rapid heating, the $\alpha \rightarrow \gamma$ phase transformation process can be modeled by a modified Johnson-Mehl-Avrami (JMA) equation for non-isothermal process. During cooling, the phase transformations are more complicated and involve not only the first order phase transformation but also displacive transformation. In this way, JMA equation would not work to predict the phase transformation during cooling. The decomposition of γ phase during cooling in the welding process has been examined by Bhadeshia et al. [2]. Given the cooling rate, their model can provide a real time quantitative description of phase constitution in the heat affected zone. In our current research, Bhadeshia's phase transformation model [2] was applied to predict the phase transformation during cooling considering the similarity of thermal cycles in the HAZ caused by laser forming and welding. Then, using the same methodology provided by Cheng and Yao [1], the flow

stress can be obtained in real time based on the phase constitution information, and the deformation can be predicted with a extensively tested thermal-mechanical finite element model [1,3].

The grain size is arguably the most important microstructural feature of a material. It contributes to the strength, ductility, toughness, corrosion resistance and other properties of the material. A quantitative understanding of the grain structural evolution during laser forming, which is mainly caused by recrystallization, is lacking up until now. The classical Johnson-Mehl-Avrami-Kolmogorov analysis [4] works well for most solid state transformation, but fails regularly when applied to model recrystallization of plastically deformed metals (i.e. during laser forming). Some attempts to simulate recrystallization with Monte Carlo techniques were also made. For instance, Srolovitz et al. [5] modeled recrystallization with both homogeneous and heterogeneous nucleation and growth using Monte Carlo technique, but the nucleation rate was assumed to be constant or site saturated, which is not realistic for the laser forming process. In the current work, the recrystallization process after inhomogeneous deformation is considering the variable nucleation rate with different temperature and strain using Monte Carlo simulation.

The objective of this work is to present a comprehensive thermal-microstructural-mechanical model to predict the deformation and microstructural evolution during complex laser forming processes. To validate the theoretically predicted results, a series of carefully controlled experiments are also conducted. The experimental and numerical results are in close agreement.

2. Mathematical Modeling

2.1 Flow stress modeling

During laser forming, phase transformation takes place in the HAZ and each present phase also undergoes work hardening and softening of dynamic recovery and recrystallization. Therefore, the strategy to model flow behavior is to calculate the flow stress of each single phase, which is influenced by the dynamic recovery and recrystallization, and then sum up the contribution of each phase by the rule of mixtures:

$$\sigma_{total} = \sum_{j=1}^{N} X_j \sigma_j \qquad (1)$$

where σ_{total} is the total flow stress, and X_j and σ_j are the volume fraction and the flow stress of the jth phase of the material, respectively. The volume fraction X_j was determined by the phase transformation model, which will be introduced later.

When strain is less than the critical strain ε_c, only work hardening and dynamic recovery exist. The classical approach to model flow stress in the regime uses the following expression [6]:

$$\sigma^{rec} = [\sigma_{ss}^{*\,2} + (\sigma_0^2 - \sigma_{ss}^{*\,2})e^{-\Omega\varepsilon}]^{0.5} \qquad (2)$$

where σ^{rec} represents the flow stress in the dynamic recovery regime, σ_0 is the initial stress, σ_{ss}^{*} is the imagined steady state stress when strain is infinite, Ω represents the ease of dynamic recovery and ε is the strain. The values of all the parameters for different phases and ε_c are adopted from the earlier paper [1].

The recrystallization takes place if the strain is larger than ε_c. The flow stress is calculated by the equation [1]:

$$\sigma = \sigma^{rec} - [\sigma_{ss}^{*\,2} - \sigma_{ss}^{rex}][1 - \exp(-K_d (\frac{\varepsilon - \varepsilon_c}{\varepsilon_{0.5} - \varepsilon_c})^{n_1})] \qquad (3)$$

where σ_{ss}^{rex} is the steady state stress after recrystallization has progressed through the material, $\varepsilon_{0.5}$ is the strain corresponding to 50 % softening due to dynamic recrystallization, and K_d and n_1 are constants. Similarly, the values of those parameters are obtained from reference [1].

2.2 Phase transformation modeling

2.2.1 α → γ transformation during heating

In the rapid heating during laser forming, the α → γ transformation in low alloy steels involves the nucleation of γ phase from the α matrix and the growth of γ phase by diffusion. Therefore, the JMA equation is applicable to describe the α → γ transformation in AISI 1010 steel. This equation is expressed as:

$$f(t) = 1 - \exp[-(kt)^n] = 1 - \exp[-\{k\sum_{i=1}\Delta t_i\}^n] \qquad (4)$$

where f stands for the transformed volume fraction of γ phase, t is the time, the JMA time exponent n is a constant independent of temperature and its value is determined by the nucleation and growth mechanism, Δt_i is time step of step i, and k is the rate factor and a function of temperature, which can be calculated by the Arrhenius equation:.

$$k = k_0 \exp(-\frac{Q}{RT}) \qquad (5)$$

where Q is the activation energy of the transformation, which does not change significantly with the variation of carbon and alloy concentrations, k_0 is the pre-exponential constant, R is the universal gas constant, and T is the absolute temperature. The temperature field and thermal cycles are calculated from the extensively tested FEM thermal modeling of laser forming. The values of constants Q, n and k_0 have been

used as 117.07 KJ mol^{-1}, 1.9 and 1.33×10^5 respectively in the welding of AISI 1005 steel [7]. Considering the similarity of the material composition between AISI 1010 steel and 1005 steel as well as the insensitiveness to temperature of those parameters, these values were used in the present investigation.

2.2.2 γ phase decomposition during cooling

The γ phase decomposition during cooling was modeled by the phase transformation model provided by Bhadeshia [2]. In the model, the time-temperature-transformation (TTT) and continuous cooling transformation (CCT) diagrams were first calculated based on thermodynamics and phase transformation kinetics. Based on the calculated cooling rate, the produced phases and their volume fractions were then determined. The model can predict the phase transformations of not only Widmanstatten ferrite and allotriomorphic ferrite, but also pearlite, bainite, and martensite. The model's details [2] assumptions, salient features, and recent applications [7] are available in the literature.

Due to very high cooling rates in the involved cases, martensite may be the dominant phase after laser scanning. In Bhadeshia's model [2] the amount of martensite $V_{\alpha'}$ is calculated by an empirical formula: [8]

$$V_{\alpha'} = (1 - V_M)[1 - \exp\{-0.011(M_s - T)\}] \qquad (6)$$

where V_M is the volume fraction of microphases, which can be estimated as in Bhadeshia et al.[2].

2.3 Monte Carlo recrystallization simulation

The Monte Carlo (MC) recrystallization simulations were carried out on 2-D cross section sites perpendicular to the scanning directions with rectangular arrangements of the lattice. Initially, the orientation numbers, $1 \leq Sg \leq 24$, were randomly assigned to each lattice site. Meanwhile, at each Monte Carlo step, some new orientation numbers ($25 \leq Sr \leq 32$), which represent the new nuclei, were randomly selected as the sites in the recrystallized region. The number of new nuclei was obtained from the calculated nucleation rate. Lattice sites, which are adjacent to neighboring sites having different grain orientations, are regarded as being part of the grain boundary, while a site surrounded by sites with the same grain orientation is regarded as being in the grain interior. In the MC simulation, the sites are visited in a random manner. Each selected site attempts to reorient to the orientation state of one of its nearest neighbors. The success of a reorientation attempt of the site depends on the energy change of the site's local configuration. The local energy state is determined using the expression [9]:

$$E = E_D f(S_i) + \sum_{j=1}^{m} J(1 - \delta_{S_i S_j}) \qquad (7)$$

where $f(S_i)$ is a step function that is unity for unrecrystallized units and zero for recrystallized units, m is the total number of the nearest neighbors of unit i (m = 8), $\delta_{S_i S_j}$ is the Kronecker delta function, S_i is the orientation at a randomly selected site i, S_j is the orientation of its nearest neighbors, J is the unit of grain boundary energy, and E_D is the stored energy. An analytical expression of stored energy was obtained by fitting to experimental results as [10]:

$$E_D = \frac{\pi}{2\overline{L}} \gamma_s \qquad (8)$$

where E_D is the stored energy, γ_s the low angle grain boundary energy, typically in the order of $\gamma_s = 0.5$ J/m^2, $\overline{L}$ is the mean linear intercept of subgrains in meters, $\overline{L} = (3.5 + \frac{1.7}{\varepsilon}) \times 10^{-7}$, and ε is the true strain.

If the local energy decreases upon reorientation, the reorientation of the unit is effectuated. If the local energy increases with the new orientation, the unit reorients or keeps its orientation with equal probability:

$$P = \begin{cases} 1 & \text{for} \quad \Delta E \leq 0 \\ e^{-\frac{\Delta E}{k_B T}} & \text{for} \quad \Delta E > 0 \end{cases} \qquad (9)$$

During laser forming, only the area close to the scan line obtains high temperature and produces large strain. Temperature and strain distribute non-uniformly; therefore, the nucleation is inhomogeneous. The inhomogeneous nucleation rate at any position $\dot{N}_a$, can be calculated by the following equation [9]:

$$\dot{N}_a = C_0 \gamma_s \left(\frac{\varepsilon}{2.2\varepsilon + 1.1} - \frac{\varepsilon_C}{2.2\varepsilon_C + 1.1} \right) \exp\left(-\frac{Q_N}{RT}\right) \qquad (10)$$

where ε_C is critical strain, generally in the range from 1 to 5 % and for low carbon steel, the critical strain is set here to 2%, Q_N is the activation energy for nucleation (the value is 18, 812 J/mol for low carbon steel [1]), and C_0 is a constant. In this case, the strain field and temperature field on the cross section are calculated from the FEM thermal-mechanical modeling of laser forming.

3. Simulation and Experiments

3.1 Modeling Procedure

To systematically predict the laser forming process based on the coupled thermal-microstructural-mechanical modeling, the mathematical models described in the previous three sections need to be rationally arranged. Fig. 1 shows the flow chart of the integration of these models.
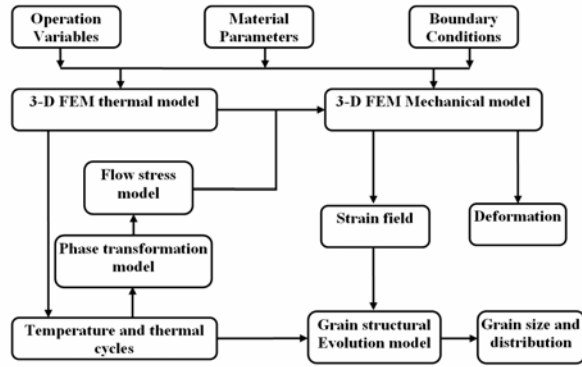

Fig. 1 Flow chart of the coupled thermal microstructural- mechanical modeling approach.

The heating and deformation during laser forming are both symmetrical about the laser scanning path; therefore only half of the plate ($80 \times 40 \times 0.89$ mm^3) is modeled in the current research. More details about the sequentially coupled thermal-mechanical modeling of laser forming can be found in references [1,3], in which the temperature dependent flow stress data came from experiments. The temperature field and thermal cycle are calculated from the 3-D thermal FEM modeling, and then the calculated temperature is input into the phase transformation model to get the volume fraction of each phase at a given time step. Because the phase transformation model and grain evolution model require very fine grids to assure enough accuracy, all phase transformation and grain evolution simulations are only carried out on a cross section perpendicular to the scanning path of the plate. This is reasonable considering that all points along the scanning direction undergo similar thermal cycles and deformations. The flow stresses are calculated based on the phase volume fractions from phase transformation modeling. Finally, the temperature field and flow stresses are input into the mechanical model to calculate the thermal strain and predict the deformation. Meanwhile, both the temperature field from the thermal modeling and the strain field from the mechanical modeling enter the grain structural evolution model as input data to describe the grain evolution during the laser forming.

Two cases were run in the current research: P = 800 W & V = 50 mm/s, and P = 400 W & V = 25 mm/s, where P represents power and V is scanning velocity.

In both cases, the laser beam spot size is 4mm in diameter.

3.2 Experiment

To validate the theoretical models, a series of carefully controlled experiments were conducted. AISI 1010 steel plates of $80 \times 80 \times 0.89$ mm^3 were laser scanned straight along the center line under different conditions: 800W & 50mm/s and 400W & 25mm/s, maintaining spot size 4 mm diameter. To enhance laser absorption by the plates, a graphite coating was applied to the surface exposed to the laser. The laser system used was a PRC 1.5 kW CO_2 laser with TEM_{00} mode. After scanning, the bending angles of the formed plates were measured by a coordinate-measuring machine (CMM). The plates were cross-sectioned perpendicular to the scanning path, polished and etched. The changes of macro and micro structures in the HAZ were observed under scanning electron microscopy (SEM). Finally, the Vickers microhardness was measured at points along the thickness of the HAZ on the scanning path.

4. Results and Analysis

4.1 Macro- and Microstructures from Experiments

Fig. 2 shows the SEM images of the laser formed cross section perpendicular to the scanning path. A distinctly darkened region is observed. The darkened sub-region immediately below the top surface is the heat affected zone (HAZ), where phase transformation took place but no melting was involved. Because the HAZ experienced high temperature and deformation, significant recrystallization took place. Both recrystallization and phase transformation caused refined grains in the HAZ. In addition, different from most thermomechanical processes, the typical thermal cycle experienced during the laser forming was very steep, which meant that the time for grain growth was severely limited. As a result, the grains in HAZ were visibly refined. Although the input line energy (P/V) was same for the two cases, the time for heat dissipation was longer with the slower scanning velocity. Thus, the case with the higher power and faster velocity (800 W & 50 mm/s) achieved a higher peak temperature and a larger HAZ.

Fig. 3 shows the grain size distribution at the top and bottom of the HAZ under the conditions of 400W & 25mm/s. The top of the HAZ experienced the highest temperature, largest deformation, and thus, the fullest extent of recrystallization. Down to the bottom of the HAZ, the extent of recrystallization is gradually reduced. The top area if the HAZ also experienced a larger extent of grain growth during laser forming.

Both recystallization and grain growth were not complete; therefore, the difference of average grain size from top to bottom of HAZ is not evident. From the SEM image of Fig. 3 (3), the boundary of the HAZ is clearly observed and the refined grains in the HAZ are much smaller than those in the base material. In the case of 800W & 50mm/s, the SEM imagines show similar results.
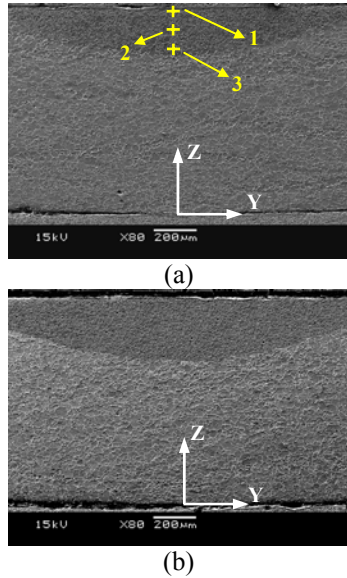

(a)

(b)

Fig. 2 The heat affected zone (HAZ) after laser scan, etched in 3% nital solution: (a) 400 W & 25 mm/s; (b) 800 W & 50 mm/s. The numbers 1, 2 and 3 in (a) represent the top, middle and bottom of the HAZ, and are consistent with the representations in the latter figures.

1

3
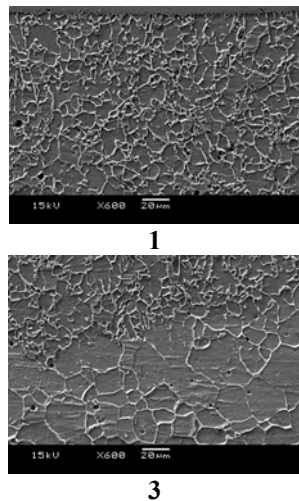
Fig. 3 The grain size distribution in the HAZ after laser scan, 400 W and 25 mm/s: 1. top of the HAZ, and 3. Bottom of the HAZ. Etched in 3% nital solution.

The phase morphology in the HAZ under the conditions of 400W & 25mm/s is shown by SEM imagines in Fig. 4. In Fig. 4 (1), lath martensite (different oriented packets with relatively parallel laths within them) is observed. Clearly, lath martensite is the dominant phase at the top of the HAZ, where the material experienced a very high cooling rate. Fig. 4 (2) shows that the lath martensite is still the main phase in the middle of the HAZ, but there exists a phase in the form of a small plate, different from retained austenite and martensite, remaining between lath martensite. This phase is thought to be the remained ferrite after the $\alpha \rightarrow \gamma$ transformation during heating. In the bottom of the HAZ, the remained ferrite increases and martensite is in the form of small laths, which can be seen from Fig. 4 (3). The case of 800W & 50 mm/s shows an identical phase distribution within the HAZ.
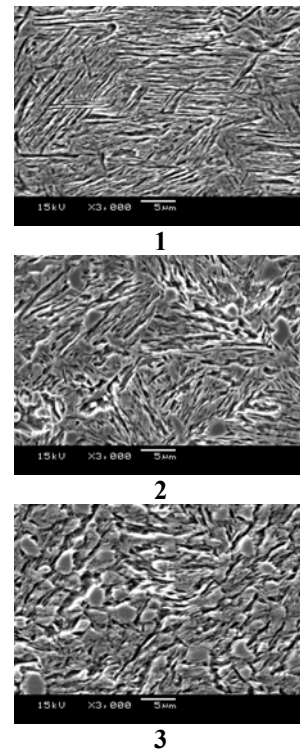

1

2

3

Fig. 4 Phase distribution of the HAZ after laser scan, 400 W and 25 mm/s: 1. top of the HAZ; 2. middle of the HAZ; and 3. Bottom of the HAZ. Etched in saturated picral solution.

Based on the experimental observation, the HAZ experienced significant recrystallization (the grain was evidently refined), and due to high cooling rate the lath martensite is substantially formed in the HAZ. The final phases in the HAZ include lath martensite, remained ferrite and a very small amount of retained austenite. The retained austenite for low carbon steel is

generally in the form of thin film between martensitic laths, and can not be observed from the SEM imagines.

4.2 Predictions by Modeling

4.2.1 Thermal Cycles

The calculated thermal cycles at thickness depths on the scanning path are shown in Fig. 5. The figure shows that the heating rate and the cooling rate are very large, and the magnitude of heating rate is up to 1×10^5 K/s. The very rapid heating and cooling would cause considerable superheating and undercooling during the laser forming. For example, the melting temperature of AISI 1010 steel under equilibrium is about 1789K, and the peak temperature in the case of 800W & 50mm/s is almost 1800K, but due to superheating, melting was not observed from SEM imagines in this case. The final microstructure is also affected by the cooling rate within the austenite decomposition temperature range. The critical cooling rate to form bainite is about 100 K/s for AISI 1010 steel [11], and from the thermal modeling, the transient cooling rate at the martensite start temperature Ms (about 700 K) is above 300 K/s. Therefore, almost all austenite is expected to form martensite during cooling, and bainite or pearlite are not produced.
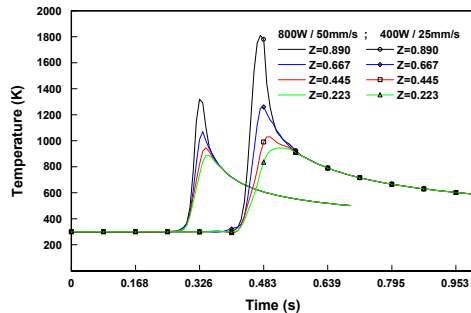

Fig. 5 The typical thermal cycles of points at different thickness depths on the scanning path (X = 20 mm, Y = 0 mm) from FEM thermal modeling of laser forming of AISI 1010 steel.

4.2.2 Phase Transformations

The phase transformation during heating is relatively simple because no melting is involved and only the α→γ transformation is considered. The process can be predicted by the JMA equation. When the heating process has just finished and the cooling process is about to start, which is assumed to be when the point at the top surface on the scanning path reaches its peak temperature, the calculated volume fractions of ferrite and transformed austenite are taken as the initial conditions for phase transformation prediction during cooling. On slow heating, the dissolution of carbides

and the formation of the γ phase take place at about 997 K for AISI 1010 steel, producing a mixture of α and γ. The α phase transforms completely to γ at about 1120 K. There is a dual phase region from 997 K to 1120 K. For the laser forming process, the dual phase region is still there, but the temperature range will shift up a little due to superheating. The calculated austenite phase distributions at the end of the heating process for both cases are shown in Fig. 6. The contours in Fig. 6 show that the HAZ region in the case of 800W & 50mm/s is larger than that in the case of 400W & 25mm/s, the same result as that of the SEM imagines. The comparison between the experimentally obtained and the calculated HAZ size is also given in Table 1. The comparison shows that the numerical result is in agreement with the experimentally obtained HAZ size.

Table.1 Comparison of HAZ size between experimental and numerical results.

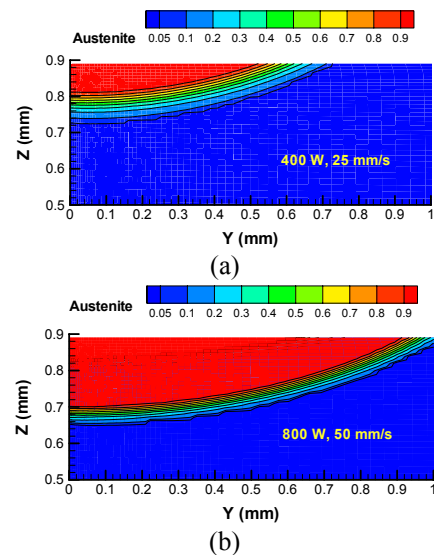|	HAZ depth (mm)		HAZ half-width (mm)	
	Exp.	Num.	Exp.	Num.
400 W & 25 mm/s	0.20	0.19	0.78	0.74
800 W & 50 mm/s	0.27	0.25	0.95	1.02

(a)

(b)

Fig. 6 The volume fraction of transformed austenite at the end of heating: (a) P = 400W, V = 25mm/s; and (b) P = 800W, V = 50mm/s.

To ensure that the values of the given material's parameters could produce the correct shapes of the γ fraction versus distance plot, the calculated distribution of transformed austenite along the thickness on the scan path was plotted in Fig. 7. The figure shows the exact exponential relationship between the phase

fraction and the distance. Fig. 7 also shows that the dual phase region in the case of 800W & 50mm/s is smaller than the 400W & 25mm/s case although the HAZ size is larger. In the case of 800W & 50mm/s, the time for heat dissipation is limited due to the faster scanning velocity and higher temperature gradient than in the case of 400W & 25mm/s. The larger temperature gradient also causes a smaller dual phase region in the case of 800W & 50mm/s.
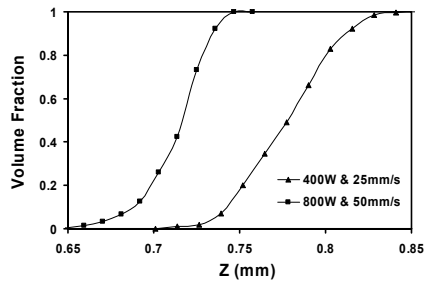

Fig. 7 The transformed austenite distribution at the end of heating along the thickness on the scan path (Y = 0 mm).

To quantitatively predict the decomposition of the γ phase in the HAZ during cooling, the cooling rates calculated from the 3D FEM thermal modeling were coupled with the Bhadeshia phase transformation model [2], which was initially applied to predict the phase transformation during welding of low carbon steel. In the present research, it was proved that the model also worked well in the laser forming having steeper thermal cycles than the welding process. The calculated phase distribution after laser forming in the conditions of 400W & 25mm/s is given in Fig. 8. From Fig. 8, almost all austenite was transformed to martensite under the very high cooling rate, and after heating the remained ferrite in the dual phase region is still there. The rest is the small amount of retained austenite (up to 3 %). As we know, the martensitic transformation can never be complete; that is, a small amount of austenite is always retained. When the carbon content of steel is high and the Ms temperature is low, a larger volume fraction of retained austenite is obtained. For AISI 1010 steel, due to its very low carbon content, only films of inter-lath austenite are retained at room temperature. The quantity of retained austenite for low carbon steel is below 4 percent. The calculated results agree well with the theoretical analysis and experimental results. Similar numerical results are obtained in the case of 800W & 50mm/s.

Fig. 9 shows the measured Vickers microhardness at various thickness depths on the scanning path. From Fig. 9, the microhardness gradually decreases down from the top of the HAZ, and there is a steep drop at the bottom of the HAZ. Hardness in the HAZ was influenced by both phase constitution and work hardening. Martensite is the phase with very high hardness, and because the volume fraction of martensite drops quickly to zero in the dual phase region, an evident drop of microhardness at the bottom of the HAZ (the dual phase region) was observed. Above the dual phase region, martensite is the dominant phase, but the region closer to the top surface experienced higher peak temperature and larger plastic deformation, and thus, has a higher hardness due to work hardening. This also provides experimental evidence for the simulated phase distribution after cooling.
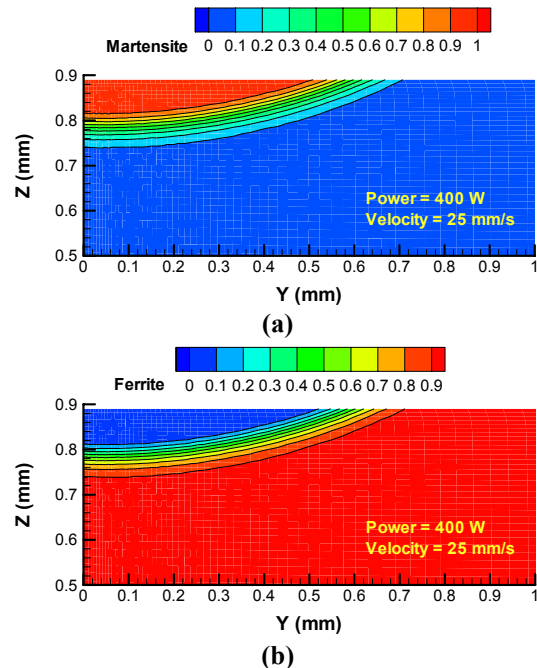

(a)

(b)

Fig. 8 The phase constitution after cooling, P = 400W, V = 25mm/s: (a). Martensite, and (b) Ferrite.
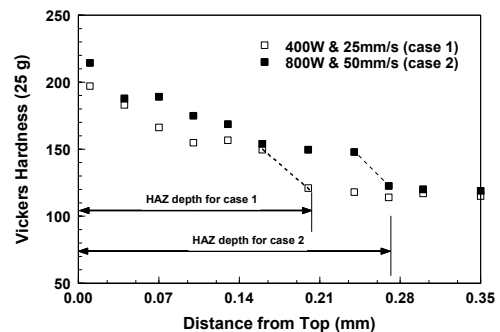

Fig. 9 The measured Vickers microhardness along thickness on the scanning path (Y = 0 mm): test load = 25g and duration time = 10s. An evident hardness drop is in the bottom of the HAZ, where the volume fraction of martensite drops quickly to zero.

From the modeling, the final phase constitution after very steep thermal cycles during laser forming includes the martensite, remained ferrite and a small amount of retained austenite. Martensite is the dominant phase in the HAZ.

4.2.3 Deformations

After the real time phase constitutive information is obtained by the phase transformation modeling, the flow behavior can be calculated by the rule of mixture (Equation. (1)). Based on the calculated transient flow stress, and the FEM mechanical modeling of laser forming, the bending angles of the plates can be predicted. Fig. 10 shows that both the experimental and the numerical results of the bending angle along the scanning path agree with each other very well. It can be seen that, from the entering end of the scanning path (X = 0 mm), the bending angle first drops a little and then increases to a greater angle at the exiting end. This phenomenon is called the edge effect and was already investigated in detail in an earlier research [3]. The drop of the bending angle after the laser enters the plate is caused by the stronger surrounding constraint in the middle of the plate. The bending edge curvature is dependent on the bending mechanism, constraint by the surrounding material and preheating. In the 400W & 25mm/s case, due to its slower scanning velocity, the exiting end was preheated to a fuller extent. Therefore, when the heat source moved from the entering end to the exiting end, the increase of the peak temperature and the thermal expansion was larger. As a result, the increase of the bending angle in the exiting end was larger than that of the 800W & 50mm/s case. Also, the bending edge curvature in the case of 400W & 25mm/s was larger.
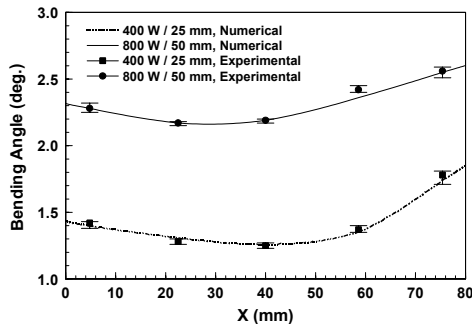

Fig. 10 The comparison between numerically predicted bending angles and experimentally obtained bending angles at different locations along scanning path (Y = 0 mm).

Fig. 11 shows the simulated history of the Y-component of the plastic strain at different points along the thickness on the scanning path. As seen, the plastic strain is severely compressive at the top surface of the

plate and slightly compressive on the lower surface. These results are easily understood. During heating, both the top and bottom of the plate tended to thermally expand, but the thermal expansion was restricted by the surrounding material, which led to the compressive plastic strain at the stage of cooling. The top was heated to a higher temperature and had a stronger tendency to expand; therefore, more compressive plastic strain was produced due to the restriction from the surrounding material, which makes the plate bend towards the laser. Meanwhile, it should be noted from Fig. 11 that plastic deformation was mainly produced in the upper region close to top the surface, and thus recrystallization only took place in the upper region on the scanning path.
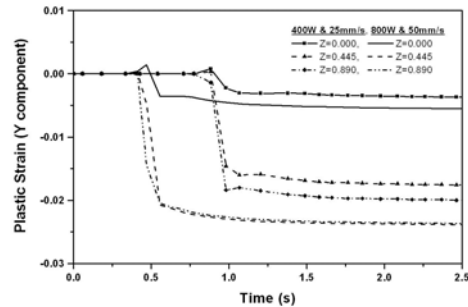

Fig. 11 Y-component of plastic strain along thickness on the scanning path (X = 20 mm and Y = 0 mm) from FEM mechanical modeling of laser forming of AISI 1010 steel.

4.2.4 Grain Size

Using the temperature and strain fields from the FEM thermal and mechanical modeling, the recrystallization process was modeled through Monte Carlo techniques. Relative to recrystallization, the contribution to grain refinement from martensitic phase transformation is much smaller, so the grain refinement caused by phase transformation is not considered in the model. Fig. 12 shows the simulated grain size and distribution, and the colors represent different grains. From the simulated results, the grain size in the HAZ is evidently smaller than that of the base material. However, the difference of grain size in the HAZ is not clearly shown from Fig. 12. Fig. 13 gives the detailed comparison of the grain size distribution in the HAZ between experimental and numerical results. The grain size measured along the thickness agrees well with the numerical results obtained. The measurements are made in a small area around a specific location, and all the measured values are averaged to get the average grain size at the specific location. The normalized grain size is the value of the local average grain size divided by the average grain size of base material. Since both the experimental and simulated microstructures were

evaluated in the same way, the agreement demonstrated in Fig. 13 indicates that, under the given conditions, the grain refinement during laser forming can be well predicted by the Monte Carlo model.
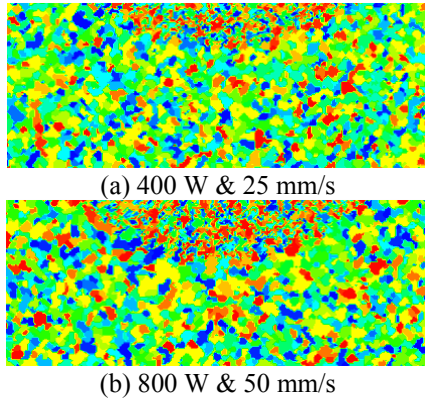

(a) 400 W & 25 mm/s

(b) 800 W & 50 mm/s

Fig. 12 The Monte Carlo modeled grain structure after recrystallization and grain growth during laser forming: (a) 400 W & 25 mm/s, and (b) 800 W & 50 mm/s.
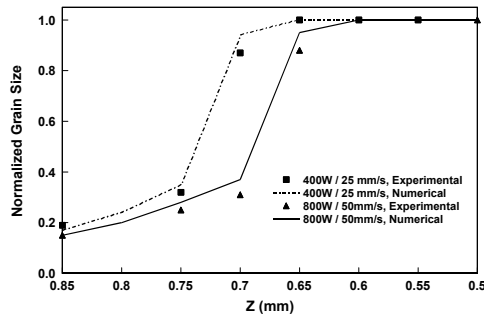

Fig. 13 The comparison between numerically predicted grain size and experimentally measured grain size at different locations along different thicknesses on the scanning path (Y = 0 mm).

5. Conclusions

A coupled thermal-microstructural-mechanical model has been developed for the laser forming process. The model considers the effect of phase transformation, work hardening, dynamic recovery and recrystallization on the deformation occurring during the laser forming process. The phase transformation of AISI 1010 steel during heating was modeled by the modified JMA equation, and the austenite decomposition during cooling was predicted by the Bhadeshia's phase transformation model, which was initially applied in the welding process. In addition, the final grain size and distribution were predicted using the Monte Carlo technique. All the numerical results agree well with the experimental results.

The simulation and direct observations of the microstructure and deformation lead to the following conclusions:

(1) Under typical thin plate laser forming, a substantial amount of martensite is formed due to the extremely high cooling rate present after the laser scan.

(2) Due to phase transformation and significant recrystallization caused by high temperature and deformation in the HAZ, the grain is distinctly refined;

(3) According to comparison of the HAZ macrostructure, phase constitution, bending angle, grain size and distribution between the experimental and numerical results, the proposed coupled model is able to accurately predict the microstructure evolution and the deformation caused through laser forming.

6. Acknowledgement

7. References

[1] Cheng, J. & Yao, Y. L. (2002) Microstructure Integrated Modeling of Multiscan Laser Forming, ASME J. Manuf. Sci. Eng., 5, 379-388.

[2] Bhadeshia, H. K. D. H., Svensson, L. -E. & Gretoft, B. (1985) Model for The development of Microstructure in Low-alloy Steel (Fe-Mn-Si-C) Weld Deposits," Acta Metall., 1271-1283.

[3] Bao, J. and Yao, Y. L. (1999) Study of Edge Effects in Laser Bending, in Proceeding ASME IMECE 1999, Nashville, TN, USA, 941-948.

[4] Humphreys, F. J. & Hatherly, M. (1995) Recrystallization and Related Annealing Phenomena, Elsevier Science, Oxford.

[5] Srolovita, D. J., Grest, G. S. & Anderson, M. P. (1986) Computer Simulation of Recrystallization – I. Homogenous Nucleation and Growth, Acta Metall., 9, 1833-1845.

[6] Harford, W. F. & Caddle, R. M. (1983) Metal Forming-Mechanics and Metallurgy, Prentice Hall, NY.

[7] Zhang, W., Elmer, J. W. & DebRoy, T. (2002) Modeling and Real Time Mapping of Phases During GTA Welding of 1005 Steel, Mat. Sci. Eng., 320-325.

[8] Trivedi, R. (1970) Growth of Dendritic Needles from a Supercooled Melt, *Acta Met*, 3, 287-296.

[9] Song, X., Rettenmayr, M., Muller, C. & Eckartexner, H. (2001) Modeling of Recrystallization after Inhomogeneous Deformation, Metall. Mater. Trans. A, 9, 2199-2206.

[10] Radhakrishnan, B., Sarma, G. B. & Zacharia, T. (1998) Modeling The Kinetics and Microstructural Evolution during Static Recrystallization – Monte Carlo Simulation of Recrystallization, Acta Metall. Mater., 4415-4433.

[11] Boyer, H. E. & Gray, A. G. (1977) Atlas of Isothermal Transformation & Cooling Transformation Diagrams, American Society for Metals.

Meet the Authors

Yajun Fan is a Ph.D candidate in the department of Mechanical Engineering at Columbia University. He received a MS in Materials Science from the Pennsylvania State University in 2002.

Zhishang Yang is a senior R&D engineer in Technology and Solutions Division at Caterpillar Inc. He received his Ph.D. from the Pennsylvania State University in 2000.

Peng Cheng is a Ph.D candidate in the Department of Mechanical Engineering at Columbia University. He received a BS in 1997 and a MS in 2000 in Mechanical Engineering from Tsinghua University, China.

Keith Egland is a manufacturing R&D supervisor within the Technology and Solutions Division at Caterpillar, Inc. He received his Ph.D. in Materials Science and Engineering from the University of Illinois at Urbana-Champaign.

Y. Lawrence Yao is a Professor in the Department of Mechanical Engineering at Columbia University. He received his Ph.D. from the University of Wisconsin-Madison in 1988. He serves on the Board of Directors of LIA.